Conformational Properties of and a Reorientation Triggered by Sugar−Water Vibrational Resonance in the Hydroxymethyl Group in Hydrated β-Glucopyranose

Teppei Suzuki,* Hirotaka Kawashima, and Takayuki Sota

Integrative Bioscience and Biomedical Engineering, Graduate School of Science and Engineering, Waseda University, 3-4-1 Okubo, Shinjuku, Tokyo 169-8555, Japan

Received: June 6, 2005; In Final Form: September 22, 2005

In this paper, we discuss the conformational properties of the hydroxymethyl group of β-glucopyranose in aqueous solution and its reorientation mechanism. First, using the values for the hydroxymethyl torsion (O5−C5−C6−O6) angle obtained by our ab initio simulations, we reestimate the experimental ratio of the hydroxymethyl rotamer populations. The reestimated ratio is found to be in agreement with those previously reported in several computational studies, which probably partly explains the discrepancies between theoretical and experimental studies that have been discussed in the literature. Second, our time-frequency analysis on a reorientation in the hydroxymethyl group in an ab initio molecular dynamics trajectory suggests that, before the reorientation, the O6−H6 stretching mode is vibrationally coupled with a proton-accepting first-hydration-shell water molecule, whereas the C6−O6 stretching mode is vibrationally coupled with a proton-donating one. The amount of the total vibrational energy induced by these vibrational couplings is estimated to be comparable to typical values for the potential barriers between hydroxymethyl rotamers. To elucidate the vibrational couplings, we investigate the hydrogen-bonding properties around the hydroxymethyl group during the pretransition period. The implications, validity, and limitation of a possible reorientation mechanism based on these findings are also discussed.

Introduction

Understanding the conformational properties of monosaccharides in aqueous solution is crucial to understanding the biological activities of oligo- and polysaccharides composed of glycosidic linkages. Among the conformational properties of monosaccharides, hydroxymethyl rotamer populations are closely related to the structures and biological functions of (1→6)-linked oligo- and polysaccharides, through the 1→6 glycosidic linkage that, unlike other linkages, has an additional torsion angle (an example of these compounds is amylopectin, which is composed of 1→4 and 1→6 linkages). Moreover, understanding the three-dimensional structures and biological functions of carbohydrates is also essential for elucidating the mechanism of molecular recognition, which may lead to the development of carbohydrate-based therapeutics.

Because of these reasons, numerous studies have addressed hydroxymethyl rotamers of carbohydrates. Among experimental techniques, an important tool for probing the conformational properties of carbohydrates in solutions is NMR spectroscopy.[1,2] ^{1}H NMR analysis of the hydroxymethyl rotamer populations for glucopyranose shows that, in aqueous solution, the gauche−trans (gt or G^+) and gauche−gauche (gg or G^-) rotamers are almost equally populated whereas the population of the trans−gauche (tg or T) rotamer is negligible.[3] However, the limiting values of vicinal proton−proton coupling constants ($^3J_{H5,H6}$) used for determining hydroxymethyl rotamer populations have been sometimes problematic, often yielding negative populations of the tg conformers.[3b,4] Recently, Stenutz et al. theoretically obtained new Karplus-type equations;[5] it was noted that the new equations are superior to the widely used the empirical Haasnoot−Altona[6] curves.[5,7,8]

A number of computational studies have also focused on the relative energies of hydroxymethyl rotamers and provided valuable insights into the conformational properties.[9−25] However, the discrepancies between theoretically determined ratios for the hydroxymethyl rotamer populations and the experimentally determined one by Nishida et al.[3] have been pointed out in the literature. First, the tg conformer of glucopyranose is actually observed in classical and ab initio molecular dynamics (MD) simulations in the aqueous phase.[26,27] Second, the gt rotamer population is estimated to be somewhat larger than the gg rotamer one,[12,18,21,25] in contrast to the experimental data. These discrepancies are still not well understood.

In addition to this, the underlying mechanism of how the hydroxymethyl group changes its orientation from one rotamer to another in solution has not been adequately addressed. In this paper, we closely examine an ab initio MD trajectory that underwent the reorientation of the hydroxymethyl group of β-glucopyranose in aqueous solution. In fact, carefully monitoring ab initio MD trajectories is a great help for understanding microscopic mechanisms, for example, elucidating the transport mechanisms of hydrated protons and hydroxyl ions in aqueous solution.[28−30] Herein, in scrutinizing the trajectory, we use a time-frequency analysis tool based on the maximal-overlap discrete wavelet packet transform[31] and the Hilbert transform, a combination of which is very similar to the Hilbert−Huang transform[32] (HHT). This kind of analysis offers the possibility to monitor how instantaneous frequencies and amplitudes of molecular motions (e.g., stretching modes) evolve in time, which is greatly helpful for elucidating the underlying mechanism. The present work will in turn provide better insights into dynamical aspects of hydroxymethyl rotamers in monosaccharides in water.

* Author to whom correspondence should be addressed. E-mail: teppei_suzuki@moegi.waseda.jp.

10.1021/jp052993z CCC: $33.50
Published on Web 01/17/2006

While ab initio MD simulations suffer from time scale problems compared with classical MD simulations, sugar−water interactions are often difficult to model by force-field parameters;[33] actually, microscopic polarization effects induced by the interactions between the OH groups of a monosaccharide and water molecules in the first hydration shell are relatively strong, as Suzuki and Sota recently showed.[34] Since the present work mainly analyzes the glucose−water interaction, this would, to some extent, justify our use of ab initio MD simulations, in which interatomic potentials are derived from electronic structure calculations based on density functional theory.[35,36] In fact, the methodology of ab initio MD is a powerful tool for studying complex systems in an accurate, unbiased way, because this methodology is substantially free from adjustable parameters.[37]

This paper is organized as follows: In the second section, we provide computational details of our simulations and briefly review the basic ideas of the HHT and the maximal-overlap discrete wavelet packet transform decomposition. In the third section, we investigate the conformational properties of the hydroxymethyl torsion (O5−C5−C6−O6) angle considering several conformers and reestimate the experimental ratio of the hydroxymethyl rotamer populations for β-glucopyranose, using the Karplus equations theoretically obtained by Stenutz et al.[5] and the values of the *J*-coupling constants reported by ^{1}H NMR spectroscopy.[3] The reestimated ratio is found to be in agreement with those determined by several computational studies and a recent NMR study, which probably partly explains the discrepancies between theoretical and experimental studies that have been discussed in the literature.[12,18,21,25−27] Also, we closely examine a reorientation in the hydroxymethyl group in an ab initio MD trajectory, using time-frequency analysis. The analysis suggests resonant vibrational couplings of the C6−O6 and O6−H6 stretching modes with first-hydration-shell water molecules, before the reorientation. Then, within these analyses, we discuss a possible reorientation mechanism for the hydroxymethyl rotamers in β-glucopyranose in aqueous solution as well as its limitations. In the last section, we summarize the conclusions and biochemical implications.

Simulation Models and Methods

Ab Initio Molecular Dynamics. The electronic structure calculations were carried out within the Kohn−Sham formulation of density functional theory. For the exchange-correlation functional, we used the gradient-corrected BLYP functional.[38] The valence−core interactions were treated by pseudopotentials by Goedecker, Teter, and Hutter.[39] Only the Γ point was used to sample the Brillouin zone. The mass of deuterium was not used for hydrogen. Our ab initio MD simulations of β-glucopyranose in aqueous solution were performed using the CPMD code.[40] The system of glucopyranose and water was modeled in a cubic supercell with sides 12.54 Å in length with periodic boundary conditions, containing 60 water molecules and 1 β-glucopyranose. In the simulations, we considered the orientations of the hydroxymethyl group and the O6−H6 group (see Figure 1 for the atomic labeling scheme). Hereafter, we refer to the rotamers associated with the former torsion angle as G^+, G^-, and T, whereas we refer to those associated with the latter torsion angle as g^+, g^-, and t.

With the above notations, we denote the starting conformations in our simulations as follows: (i) G^+g^+, (ii) G^+t, (iii) G^+g^-, (iv) G^-g^+, (v) G^-t, and (vi) Tg^-. In simulations i−iii, v, and vi, we used a cutoff energy of 70 Ry, a time step of 0.0968 fs, and a fictitious electronic mass of 400 au,[41] whereas in simulation iv, we used a cutoff energy of 80 Ry, a time step of 0.0822 fs, and a fictitious mass of 340 au. The MD trajectories were sampled at every 10 steps. In all of the simulations, the Nosé−Hoover chain thermostat method[42,43] was used to control the ionic temperature at 300 K for equilibration. In simulation i, after an initial equilibration phase of 3 ps, data were collected for a microcanonical MD run of 8.2 ps. In each of the simulations ii, iii, v, and vi, after an initial equilibration phase of 3 ps, data were collected for a microcanonical MD run of 6 ps. In simulation iv, data were collected for a microcanonical MD run of 10 ps, after an equilibration phase of 6 ps. Note that, in the present work, we mainly scrutinize the ab initio MD trajectory obtained by simulation i, which experienced reorientations of the hydroxymethyl group. In simulations ii−vi, the initial conformations about the two torsion angles were maintained to the end of the simulation runs.

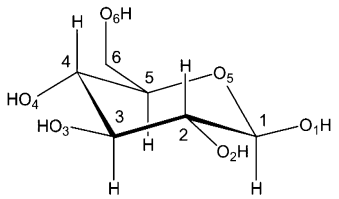

Figure 1. Atom labeling scheme for β-glucopyranose. The orientations for the O5−C5−C6−O6 torsion angle are normally denoted by G^+, G^-, and T (ideally, +60°, −60°, and 180°, respectively), whereas those for the C5−C6−O6−H6 torsion angle are denoted by g^+, g^-, and t, (ideally, +60°, −60°, and 180°, respectively) in this paper. G^+, G^-, and T are identical to the most widely used notations, gt, gg, and tg, respectively.

Time-Frequency Analysis. Time-frequency analysis using the HHT has been applied for a variety of systems including fluid mechanics,[44] chaotic systems,[45] molecular dynamics simulations,[46,47] and epidemiology.[48] In the method of empirical mode decomposition (EMD) proposed by Huang et al.,[32,44] an original signal is decomposed into several intrinsic mode functions (IMFs) that are suited for the calculation of instantaneous frequencies via the Hilbert transform, and a residue, using a sifting process. While these IMFs are often physically meaningful, it was originally noted that this does not necessarily hold, in particular, for the situations where decomposed components contain more than one characteristic frequency.[32,44] This is probably due to the algorithm of the EMD method, in which IMFs are decomposed from the highest- through lowest-frequency components.

Recently, Olhede and Walden proposed that EMD can alternatively be replaced by another decomposition method based on the discrete wavelet packet transform (DWPT) for the calculation of instantaneous frequencies.[49] In the DWPT, a frequency region between zero and the Nyquist frequency is divided into 2^j equal-width subbands ($j = 0, 1, 2, ...$). Here, j is called the *level* of decomposition. In the conventional DWPT, the phases of decomposed components are shifted from an original time series, at every increase of the level. This feature reduces the possibility of practical applications of the DWPT. However, Walden and Contreras Cristán recently showed that this bottleneck is circumvented by introducing *cyclic filtering steps*;[50] this modified version of the DWPT is called the *maximal-overlap* discrete wavelet packet transform (MODWPT). Unlike the conventional DWPT, the *detail coefficients* and the *smooth coefficient* obtained by the MODWPT (which correspond to IMFs and a residue in the framework of EMD, respectively) are associated with zero-phase filters.[31,50] Therefore, all detail coefficients line up completely with the features of an original time series at any *j*th level. However, the phases of the *raw* MODWPT coefficients are still shifted from the

features of the original time series, at every level increase, even in the framework of the MODWPT.[31,49] However, the former outstanding feature is appropriate for our Hilbert-transform-based time-frequency analysis because, in calculating instantaneous frequencies via the Hilbert transform, we use detail coefficients only. What is more, another merit of the MODWPT is that any sample size can be used, instead of the power of 2.[31,49] Certainly, one might argue that whether the detail coefficients decomposed by the MODWPT satisfy the condition for IMFs is not obvious; nevertheless, in a practical meaning, they are usually well-defined monocomponent signals and thus assumed to be used for the calculation of instantaneous frequencies via the Hilbert transform.

Following Walden and co-workers,[31,49,50] we call a frequency band between $\nu_{j,n}$ and $\nu_{j,n+1}$, where $\nu_{j,n} = n\nu_{\mathrm{Nyq}}/2^j$ ($n = 0, 1, ..., 2^j - 1$), the *nth frequency band at the jth level* (where ν_{Nyq} is the Nyquist frequency, which is about 17 247 cm^{-1} in our present study). For example, the third frequency band at the sixth level ($\nu_{6,3}$) is, in our case, defined by a band between about 808 and 1078 cm^{-1}. Since each subband has one detail coefficient, the merit of the MODWPT over the EMD method is that, if a decomposed component seems to contain more than one characteristic frequency, then one can increase the level of decomposition. Furthermore, Olhede and Walden[49] also pointed out that the instantaneous frequencies obtained using the decomposed components by the MODWPT are superior to those obtained by EMD. In our present study, we used the HHT in a supplementary manner; that is, to determine the target frequency bands for the MODWPT decomposition, we evaluated the overall features of the time-frequency spectra obtained by the HHT. In the MODWPT, we used Daubechies's least asymmetric scaling and wavelet filters.[51]

Results and Discussion

In simulation i, β-glucopyranose underwent three major conformational changes about the O5−C5−C6−O6 and C5−C6−O6−H6 torsion angles (Figure 2a). First, during about 0.34−0.57 ps, the orientations of the hydroxymethyl and O6−H6 groups of the β-glucopyranose changed almost simultaneously from the G^+g^+ to the Tg^- conformer. Second, during about 4.12−4.41 ps, the orientations returned to the initial G^+g^+ conformation. Third, during about 6.12−6.52 ps, the orientation of the O6−H6 group only changed from the G^+g^+ to the G^+t conformer.

Before scrutinizing this trajectory, we evaluated the average values for the hydroxymethyl torsion angle in all of the simulations to investigate the deviations from the perfectly staggered conformations. In simulation i, the maximum peak position of the distribution of the O5−C5−C6−O6 torsion angle for the G^+ rotamer was about 63° whereas the one associated for the T rotamer was about 153° (see also the red bold solid line in Figure 2b). In simulations ii−vi, the averaged values for the O5−C5−C6−O6 torsion angles were 62.7°, 75.0°, −68.4° −59.7°, and 152.5°, respectively (these correspond to the distributions denoted by black solid, black dashed, greed solid, green dashed, and blue solid lines in Figure 2b, respectively). Independent of the orientations of the O6−H6 group, the O5−C5−C6−O6 torsional angle in the T rotamer deviated significantly from its ideal value of 180° toward the value in the G^+ rotamer and hence away from that in the G^- rotamer (Figure 2). The size of the deviation from the ideal value was about 30°. The results imply that, in β-glucopyranose in the aqueous phase, the transition between G^+ and T is probably somewhat easier than the one between G^- and T.

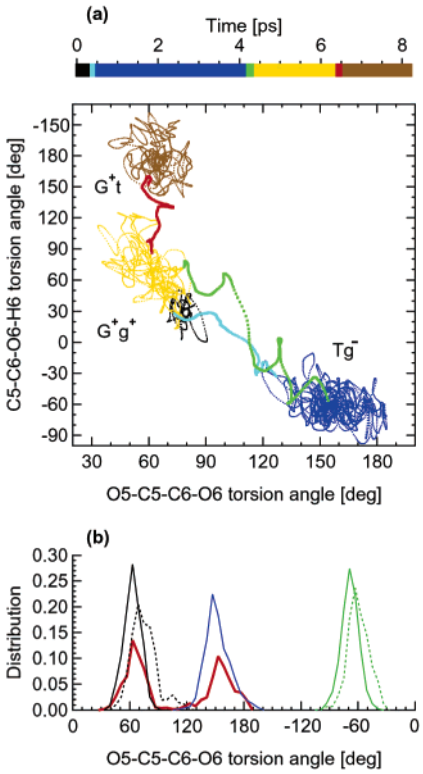

Figure 2. (a) Ab initio MD trajectory undergoing the reorientation of the hydroxymethyl group that is mapped onto the two-dimensional space defined by the O5−C5−C6−O6 and C5−C6−O6−H6 torsion angles and (b) the distributions of the O5−C5−C6−O6 torsion angles obtained by the ab initio MD simulations. In part a, each color corresponds to each state or transition: black, G^+g^+; light blue, a transition from G^+g^+ to Tg^-; blue, Tg^-; green, a transition from Tg^- to G^+g^+; yellow, G^+g^+; red, a transition from G^+g^+ to G^+t; brown, G^+t (see also the color scale in part a). In part b, shown are the distribution of the O5−C5−C6−O6 torsional angles obtained by the same ab initio MD trajectory in part a (the red bold solid line) and those obtained by the ab initio MD simulations of G^+t (the black solid line), G^+g^- (the black dashed line), G^-g^+ (the green solid line), G^-t (the green dashed line), and Tg^- (the blue solid line).

In fact, a very long (50 ns) classical MD simulation of methyl α-glucopyranoside in water recently performed by Kirschner and Woods[22] shows that the transitions between the G^+ and T rotamers occur frequently in aqueous solution whereas the conformational lifetime of the G^- rotamer is much longer (its estimated lifetime is roughly 5 ns). Moreover, their potential energy surfaces along with the hydroxymethyl torsion angle for methyl α-glucopyranoside obtained from both the quantum chemical and molecular mechanics calculations show that the position associated with the T conformer is located at ∼160°.[22] While our values (about 153°) for the O5−C5−C6−O6 torsion angle are somewhat smaller than those reported in computational studies (quantum chemical calculations in the gas phase,[52] 166−170°; an MD simulation in the aqueous phase,[19] 169°; quantum chemical/molecular mechanics calculation,[25] 171°), our results with the ab initio MD simulations are in reasonable agreement with the computational study by Kirschner and Woods. The relative positions obtained by our ab initio MD simulations (Figure 2b) and the ones reported in the above recent computational study[22] suggest that the three torsion angles of the hydroxymethyl rotamers of glucopyranose and its derivatives significantly deviate from the perfectly staggered conformations.

These kinds of deviations from the perfectly staggered conformations have been problematic when experimentally determining hydroxymethyl rotamer populations from *J*-cou-

pling constants because, in determining the six limiting values from Karplus-type equations, the torsion angles of the three hydroxymethyl rotamers are often assumed to be the ideal values (−60°, 60°, and 180°).[4] However, calculated populations of the T rotamers often yield negative values.[3b,4] To circumvent these physically meaningless populations, some authors suggested that populations of the T rotamers should be set to zero if the populations are negative,[4] while others recommended modified values for the O5−C5−C6−O6 torsion angle that are close to those obtained by X-ray experiments.[3b] It was also reported that using the torsion angles obtained by molecular mechanics for the determination of the six limiting values from Karplus-type equations improves the values for populations of the T rotamers, reasonably reducing negative populations.[53]

Recently, Stenutz et al.[5] theoretically obtained new equations for *J*-coupling constants associated with hydroxymethyl groups ($^3J_{H5,H6}$), which are a function of the O5−C5−C6−O6 torsion angle. In particular, it was shown that, when this torsion angle is near 60° and −60°, the empirical Haasnoot−Altona curves[6] slightly deviate from the new equations.[5] It was confirmed that the use of the new limiting values for $^3J_{H5,\ H6R}$ and $^3J_{H5,\ H6S}$ yield positive populations for the T conformers in the cases studied.[5] Here, with the new equations, we therefore calculated the hydroxymethyl rotamer populations for β-glucopyranose in D_2O, using the same values for *J*-coupling constants previously reported by Nishida et al.[3] ($^3J_{H5,H6R}$ and $^3J_{H5,H6S}$ are 6.0 and 2.1 Hz, respectively). When we used the perfectly staggered conformations (−60°, 60°, and 180°), we obtained a ratio of 43:56:1 for $G^-/G^+/T$ (gg/gt/tg); however, the use of the averaged values obtained by our ab initio MD simulations (−64°, 67°, and 153°; these were obtained by averaging over the values shown in Figure 2b) yielded a ratio of 31:59:10.

For comparison, we also calculated the rotamer populations using several sets of three values for the O5−C5−C6−O6 torsion angle. In general, the use of the new equations gave a greater population of the G^+ rotamer over the G^- rotamer and a 7−11% population for the T rotamer (Table S1 in the Supporting Information). The two trends are in agreement with a recent sophisticated NMR spectroscopic study and several computational studies (Table 1). In particular, the greater population of the G^+ rotamer is qualitatively consistent with a quantum chemical study by Barrows et al.,[21] a quantum chemical/molecular mechanics study by Corchado, Sánchez, and Aguilar,[25] and an MD study by Grootenhuis and Haasnoot[12] (Table 1). Furthermore, our reestimated ratio (31:59:10) is in good agreement with the theoretically determined one by Senderowitz, Parish, and Still[18] and that for methyl β-glucopyranoside that was recently experimentally determined by Thibaudeau et al.[8] (32:59:9) (Table 1). These suggest that the T conformer of glucopyranose has a small population (probably, roughly 10%) in aqueous solution and that the $G^-/G^+/T$ ratio of β-glucopyranose in aqueous solution is possibly about 30:60:10 (or about 35:55:10) rather than a ratio of about 55:45:0 that was originally estimated by Nishida and co-workers.[3] In fact, the T rotamer is observed in classical and ab initio MD simulations of glucopyranose in aqueous solution[26,27] and was observed in the present simulation as well. However, the reestimated ratio is in considerable disagreement with that by Wladkowski et al.[20] and that by Kuttel, Brady, and Naidoo.[23]

In addition, we verified that a combination of slightly increased values for the G^+ rotamer and slightly decreased values for the G^- rotamer increased the population of the T rotamer; what is more, for larger deviations, the decrease of the value for the T rotamer had an additional effect on the population of the T rotamer (Figure S1 in the Supporting Information). Note that the two torsion angles (i.e., the G^- and G^+ rotamers) of gluco configurations often slightly deviate from the perfectly staggered conformations (typically, 5−10°) both in crystalline structures[54−56] and in computer simulations in the aqueous phase.[19,53] Therefore, these suggest that reported negative populations of the T rotamer of glucopyranose derivatives in NMR studies[3b,4] are partly due to the inaccuracy of the Haasnoot−Altona curves[6] and partly due to the assumption of the perfectly staggered conformations. Presumably, these partly explain the discrepancies in the population of the T conformer between theoretical and experimental studies that have been discussed in the literature.[12,18,21,25−27] Moreover, while the lengths of our simulations are limited, our computed values for the O5−C5−C6−O6 torsion angle in aqueous solution from first principles and our analysis herein may imply that care should be taken into account when one uses the ideal values (that is, the perfectly staggered conformations) for the determination of the six limiting values of vicinal proton−proton coupling constants from Karplus-type equations in calculating hydroxymethyl rotamer populations of monosaccharides in solution.

Obviously, we note that, whereas carbohydrate samples are normally dissolved in D_2O in NMR experiments,[2] H_2O is normally used in molecular dynamics simulations and in quantum chemical calculations. However, in these computations,

TABLE 1: Comparison of Our Reestimated Experimental Ratio of the Hydroxymethyl Rotamer Populations (%) with Those Determined Theoretically and Experimentally

	rotamer population		
method	G^- (gg)	G^+ (gt)	T (tg)
GROMOS force field[a]	41	43	16
CHEAT force field[b]	25	65	10
AMBER* force field + the GB/SA continuum model for water[c]	27	63	9
CHARMM CSFF[d]	66	33	1
QM + SCIPCM[e]	67	25	8
QM + SM5.4/AM1 solvation model[f]	29	66	5
QM/MM[g]	12	83	5
	19	72	9
NMR data (methyl β-glucopyranoside)[h]	32	59	9
our reesitimated ratio using data by Nishida et al.[i]	31	59	10

[a] The relative free energies in Figure 10 in ref 11 (van Eijck et al.) were used to calculate the Boltzmann-averaged populations for β-glucopyranose. [b] Grootenhuis and Haasnoot (ref 12). [c] Senderowitz et al. (ref 18). They originally reported a ratio of 27:63:9; however, note that the sum is 99. [d] Kuttel et al. (ref 23). [e] The relative electronic energies (at the MP2/6-31G(d) level) in Table 3 in ref 20 (Wladkowski et al.) were used to calculate the Boltzmann-averaged populations for β-glucopyranose. [f] The relative free energies (at the MP2/cc-pVDZ level) in Table 3 in ref 21 (Barrows et al.) were used to calculate the Boltzmann-averaged populations for β-glucopyranose. [g] The relative free energies (at the B3LYP/6-31+G(d,p) level) in Table S11 in the Supporting Information for ref 25 (Corchado et al.) were used to calculate the Boltzmann-averaged populations for β-glucopyranose. The second entries were obtained using the relative free energies (at the MP2/6-311++G(d,p) level using the optimized structures calculated at the B3LYP/6-31+G(d,p) level) in the third column of Table S12 in the Supporting Information for ref 25. [h] Thibaudeau et al. (taken from Table 7 in ref 8). [i] With the new equations proposed by Stenutz et al. (ref 5) (the averaged values obtained by our ab initio MD simulations, −64°, 67°, and 153°, were used in determining the six limiting values), we calculated the hydroxymethyl rotamer populations for β-glucopyranose in D_2O using the values for *J*-coupling constants reported by Nishida et al. (ref 3) ($^3J_{H5,H6R}$ and $^3J_{H5,H6S}$ are 6.0 and 2.1 Hz, respectively). Note that the originally estimated ratio by Nishida et al. is 53:45:2 (ref 3).

the zero-point-energy effects of solvents are not included; therefore, within the theoretical approximation in which nuclei are treated classically, solute−solvent electrostatic interactions are identical between liquid D_2O and H_2O solvents. Hence, if we assume that the potential surface along with the hydroxymethyl rotation is primarily determined by electrostatic interactions and local arrangements of hydrogen bonds around the hydroxymethyl group and that the zero-point-energy difference between the two solvents has little effect on the hydroxymethyl conformational surface, equilibrium (averaged) values for the O5−C5−C6−O6 angle are essentially identical between liquid D_2O and H_2O solvents. Therefore, while our values for the O5−C5−C6−O6 angle were obtained using liquid H_2O solvent, the values and the reestimated ratio in Table 1 are likely to be relevant for liquid D_2O solvent.

After we had evaluated the conformational properties of the hydroxymethyl group in aqueous solution, we examined the hydration structure around O6 in the MD trajectory that underwent the reorientation of the hydroxymethyl group (simulation i). By carefully monitoring the ab initio MD trajectory, we found that three water molecules were involved in the hydration of O6: a proton acceptor and two proton donors (Figure 3a). First, we looked at the proton acceptor (hereafter, we refer to this water molecule as W_A); we found that W_A, the proton-accepting water molecule indicated by O_A in Figure 3a, continuously hydrogen-bonded with O6, even during the period of the reorientation of the hydroxymethyl group (Figure 3b), indicating that the interaction was markedly strong. In fact, Suzuki and Sota recently showed that, when a water molecule accepts a proton from an OH group of β-ribofuranose, the water molecule dipole moment is enhanced.[34] Thus, we calculated the dipole moment of W_A, using the centers of relevant maximally localized Wannier functions;[57,58] the average value during 0−6 ps was 3.17 D, being about 0.2 D larger than that of pure liquid water.[34,59] This enhancement induced by the microscopic polarization effects appeared to be the physical origin of the observed somewhat long-lived hydrogen bond (Figure 3b), which is consistent with our previous work.[34]

To investigate the role of the proton-accepting water molecule during the simultaneous reorientations of the hydroxymethyl group and the O6−H6 group, we carefully monitored the ab initio MD trajectory. The representative snapshots showing the G^+ and T conformers and the transient conformations in Figure 4 indicate that the role of W_A appeared rather simple; since, owing to the hydrogen bond with W_A, H6 was constantly pointed toward O_A during the reorientation of the hydroxymethyl group, the orientation of the O6−H6 group automatically changed. Note that, while the time evolution of the O5−C5−C6−O6 torsion angle during the transitions increased fairly linearly (0.34−0.57 ps; about 4.4° per 10 fs) or decreased (4.12−4.41 ps; about −3.8° per 10 fs), that of the C5−C6−O6−H6 torsion angle increased or decreased in a somewhat fluctuating manner, mainly because the H6 was greatly bound to W_A.

Second, we examined the two water molecules that acted as proton donors, namely, those denoted by O_{D1} and O_{D2} in Figure 3a. Hereafter, we refer to these water molecules as W_{D1} and W_{D2}, respectively. The lifetimes of the hydrogen bonds between O6 and these water molecules were not compared with that for W_A (Figures 3b−d). In fact, the average values for the dipole moments of W_{D1} and W_{D2} were 2.85 and 2.82 D, respectively. These values are slightly smaller than that of pure liquid water (2.95 D),[34,59] indicating that the dipole moments of these proton-donating water molecules were not greatly enhanced, which is basically consistent with our previous work.[34]

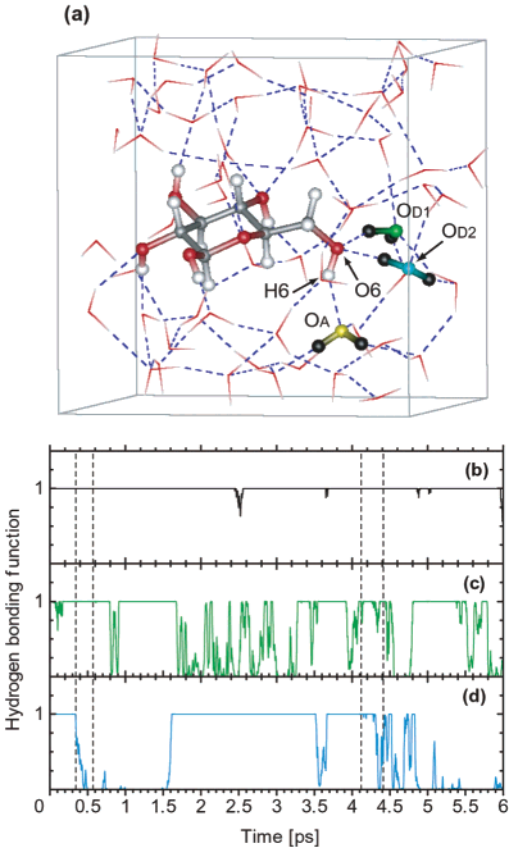

Figure 3. Three first-hydration-shell water molecules hydrogen-bonding to the hydroxymethyl oxygen (O6). In part a, a snapshot taken from the ab initio MD trajectory is shown. The dashed blue lines in part a indicate hydrogen bonds. The three water molecules are represented by ball-and-sticks, in which O_A (an acceptor), O_{D1} (a donor), and O_{D2} (a donor) are indicated separately by yellow, green, and blue, respectively, while hydrogens, by black. The other water molecules are represented by sticks, and the β-glucopyranose molecule is represented by ball-and-sticks (carbon atoms, gray; oxygens, red; hydrogens, white). For our molecular visualization, throughout the paper, we used gOpenMol, version 2.32 (ref 81). In parts b−d, we show the hydrogen-bonding functions for the hydrogen bonds between O6 and each of the three water molecules (part b, O6···O_A; part c, O6···O_{D1}; part d, O6···O_{D2}). Our hydrogen-bonding function is unity if $d(t) \leq d_c$ and otherwise $\exp(-(d(t) - d_c)^2/2\sigma_r^2)$, where $d(t)$ is the instantaneous H···O_a distance, and in our present work, d_c and σ_r were 2.2 and 0.2 Å, respectively. The dashed lines in parts b−d indicate the start and final points of the observed transitions (part c, about 0.34 and 0.57 ps; part d, about 4.12 and 4.41 ps).

Next, we looked at the time series of the C6−O6 and O6−H6 distances of β-glucopyranose. During about 3.4−3.8 ps, the amplitudes of the oscillations of the C6−O6 and O6−H6 distances were simultaneously remarkably large; in particular, the largest value for the C6−O6 distance was 1.642 Å (at ∼3.670 ps in Figure 5a). In contrast, during the transition (about 4.1−4.4 ps, from Tg^- to G^+g^+), the amplitudes of the oscillations became rather small (Figure 5). Since the hydroxymethyl oxygen (O6) was hydrogen-bonded with the three water molecules (W_A, W_{D1}, and W_{D2}) during this time region (3.4−3.8 ps in Figures 3b−d), these observations suggest that the large amplitudes of the C6−O6 and O6−H6 distances were closely related to the hydration around the hydroxymethyl group. Also, we examined these time series during −0.5−0.7 ps (where the time origin is set to the starting point of the NVE simulation) and found that the highest amplitude (1.633 Å) of the C6−O6

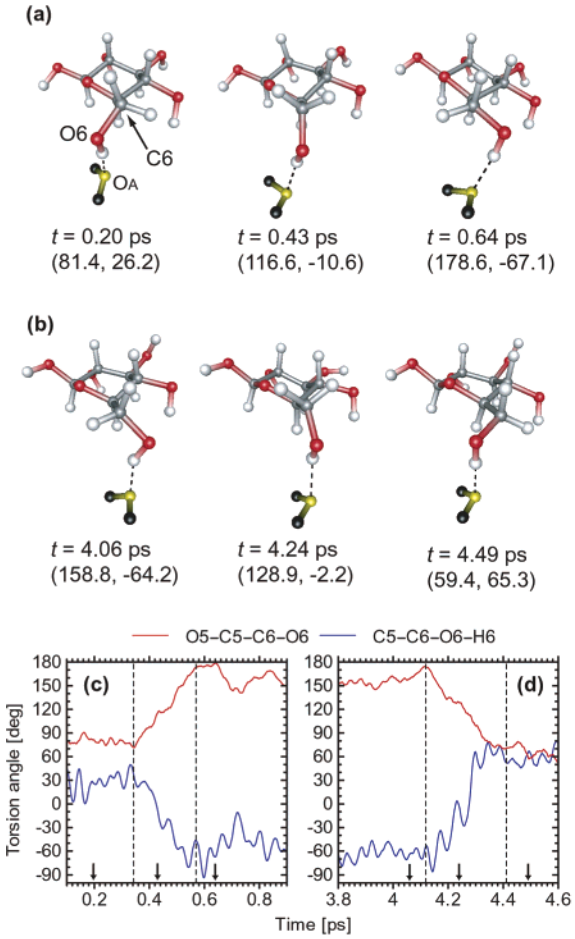

Figure 4. Role of the proton-accepting water molecule in the observed simultaneous reorientations of the O5−C5−C6−O6 and C5−C6−O6−H6 torsion angles. Parts a and b show snapshots taken from the ab initio MD trajectory undergoing the transition from G^+g^+ to Tg^- and the one from Tg^- to G^+g^+, respectively. The values in parentheses in parts a and b are the O5−C5−C6−O6 (left side) and C5−C6−O6−H6 (right side) torsion angles in degrees. In the β-glucopyranose molecule, carbon atoms are colored gray, oxygens red, and hydrogens white, whereas in the proton-acceptor water molecule, which is indicated by O_A, the oxygen is colored yellow and the hydrogens black. The other water molecules are omitted. The dashed line in parts a and b indicates the hydrogen bond between O6 and O_A. The time series of the O5−C5−C6−O6 (red) and C5−C6−O6−H6 (blue) torsion angles are also shown in the (c) 0.1−0.9 and (d) 3.8−4.6 ps regions, respectively. The dashed lines in parts c and d are the start and final points of the transitions (part c, about 0.34 and 0.57 ps; part d, about 4.12 and 4.41 ps). The arrows in parts c and d indicate the positions of the three snapshots shown in parts a and b, respectively.

stretching oscillation was located at −0.092 ps (see label A in Figure S2 in the Supporting Information). This implies that the time region needed for analyzing the mechanism underlying the transition from G^+g^+ to Tg^- is located between the NVT and NVE simulations. However, the dynamics of NVT simulations controlled by the Nosé−Hoover chain thermostat method is substantially restricted;[43] in fact, we observed that OH stretching vibrations in the NVT simulation were considerably different from those in the NVE simulation. Thus, since the dynamics during −0.5−0 ps (the NVT-simulation region) that might be associated with the transition from G^+g^+ to Tg^- does not reflect the natural dynamics, we scrutinized only the dynamics associated with the transition from Tg^- to G^+g^+ (the one during 4.12−4.41 ps).

The aforementioned observations led us to postulate that the trigger for the reorientation of the hydroxymethyl group was

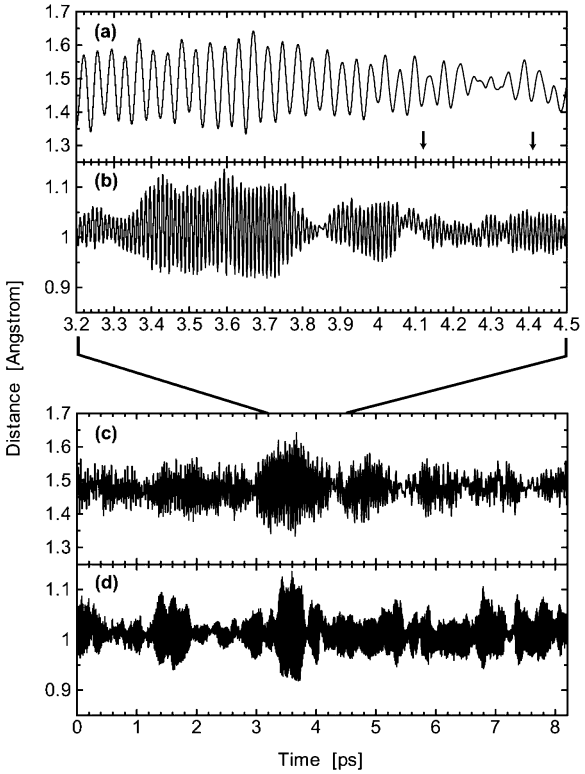

Figure 5. Time series of the C6−O6 (part a, 3.2−4.5 ps; part c, 0−8.2 ps) and O6−H6 (part b, 3.2−4.5 ps; part d, 0−8.2 ps) distances. The arrows in part a indicate the initial and final points of the transition from Tg^- to G^+g^+ (about 4.12 and 4.41 ps, respectively).

closely related to the interactions between the O6−H6 group and the three first-hydration-shell water molecules. With this perspective, we scrutinized the vibrational properties of the O6−H6 group and the first-hydration-shell water molecules, using a recently proposed time-frequency analysis tool that combines the Hilbert transform and the MODWPT.[49] Since the CPMD method within the BLYP functional typically underestimates frequencies of molecular vibrations by about 10%, a somewhat ad hoc scaling factor (which might depend on fictitious electronic masses, systems, and pseudopotentials) is necessary; in the present work, we used a scaling factor of 1.1.

The average instantaneous frequencies of the O6−H6 and H6···O_A stretching vibrations during 2−5 ps were 3405 and 3377 cm^{-1} (the instantaneous frequencies that were cut off in Figure 6 were excluded in averaging; this procedure was used for all of the similar calculations), respectively. This indicates the vibrational coupling between the O6−H6 stretching vibration with the proton-accepting water molecule. Moreover, the average O6−H6 stretching-mode frequency during 3.2−4.1 ps was 3334 cm^{-1} whereas the one during 4.1−5.0 ps was 3476 cm^{-1}; that is, the O6−H6 stretching-mode instantaneous frequencies during 3.2−4.1 ps were lower than those during 4.1−5.0 ps (Figure 6a). The former and latter frequencies correspond to stronger and weaker hydrogen bonds. Consistently, the average values for the O6···O_A distance during 3.2−4.1 and 4.1−5.0 ps were 2.799 and 2.978 Å, respectively. These suggest that, during the vibrational coupling, the hydrogen bond between O6 and W_A was relatively strong, whereas, during the reorientation, the hydrogen bond became slightly weaker.

The instantaneous average frequencies of the C6−O6 and O6···O_{D1} stretching vibrations during 2−5 ps were 956 and 968 cm^{-1}, respectively (we empirically found that EMD could not clearly decompose these signals compared with the MODWPT decomposition), which indicates the vibrational coupling be-

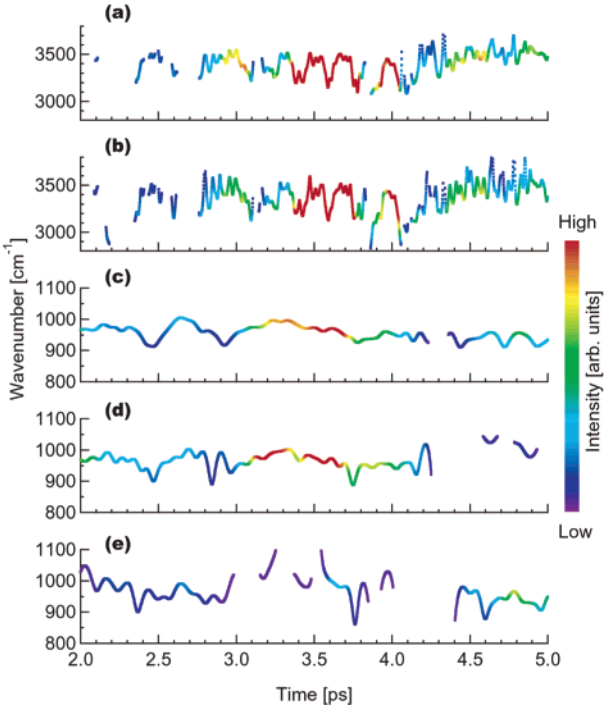

Figure 6. Time-frequency spectra in the 2−5 ps region obtained from the time series of the (a) O6−H6, (b) H···O_A, (c) C6−O6, (d) O6···O_{D1}, and (e) O6···O_{D2} distances. In parts a and b, the time-frequency spectra for the decomposed component associated with the first band at the third level are shown in the 2800−3800 cm^{-1} region (which is relevant for OH stretching vibration). In parts c−e, the time-frequency spectra for the decomposed component associated with the third band at the sixth level are shown in the 800−1100 cm^{-1} region (which is relevant for the CO stretching vibration). All spectra were obtained using the maximal-overlap discrete wavelet packet transform and the Hilbert transform (for details, see the text); in the present work, the Hilbert transform was obtained using the convolution theorem. Because of an underestimate of the CPMD method with the BLYP functional, we used a scaling factor of 1.1 for the instantaneous frequencies. A cutoff of 3% of the maximum intensities was used for all of the spectra. See also parts b and d of Figure 7 for the detail coefficients that correspond to parts d and e, respectively. For the notations O_A, O_{D1}, and O_{D2}, see Figure 3a.

tween the C6−O6 stretching vibration with W_{D1} (the proton-donating water molecule) (Figures 6c and 6d).[60,61] Therefore, our time-frequency spectra in Figures 6a−d confirm that the markedly large amplitudes of the C6−O6 and O6−H6 oscillations during 3.4−3.8 ps in Figure 5 were induced by the vibrational couplings. In contrast, the vibrational coupling between O6 and W_{D2} appeared less important (Figure 6e).

To verify the above difference in the vibrational coupling between the two proton-donating water molecules (W_{D1} and W_{D2}), we also compared the time series of the decomposed components (i.e., the detail coefficients) obtained from the time series of the O6···O_{D1} and O6···O_{D2} distances. The time evolution of the detail coefficient associated with the third band at the sixth level for the O6···O_{D1} distance ranged ±0.02 Å during 3.1−4.0 ps (Figure 7b). Note that this oscillation is slightly visible in the original time series of the O6···O_{D1} distance (Figure 7a). However, the detail coefficient for the O6···O_{D2} distance was fairly small (Figure 7d). These and Figures 6c−e suggest that the vibrational coupling of the C6−O6 stretching vibration was induced exclusively by the interaction between O6 and W_{D1}.

To clarify this point from a geometrical point of view, we examined the time series of the O6−C6−O_{D1} and O6−C6−O_{D2} angles. During 3.5−3.6 ps, the former angle was remarkably

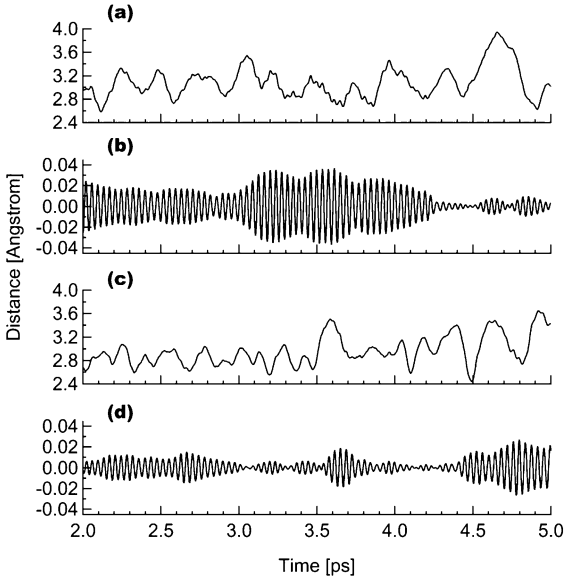

Figure 7. Time series of the (a) O6···O_{D1} and (c) O6···O_{D2} distances and the time series of their decomposed components (b and d). Time series in parts b and d are the detail coefficients associated with the third band at the sixth level (for the definition, see the text) obtained from the time series of the O6···O_{D1} and O6···O_{D2} distances, respectively. For the notations O_{D1} and O_{D2}, see Figure 3a.

small whereas the latter one was not (Figure S3 in the Supporting Information), which means that the C6−O6 and C6−O_{D1} axes were almost parallel immediately before the hydroxymethyl rotamer transition. This possibly implies that the C6−O6 stretching vibration was effectively vibrationally coupled with W_{D1}, because, in this time region, the amplitude of the C6−O6 stretching vibration was remarkably high (Figures 5a and 6c). The result also implies that orthogonal components (with respect to the C6−O6 axis) of dynamical motions between O6 and a proton-donating water molecule do not significantly interact with the C6−O6 stretching motion, which is reasonable from a simple physical point of view. This issue will be discussed later.

Within these findings, we modeled a simple but possible mechanism for the observed reorientation from the T to G^+ conformer. Our proposed mechanism consists of two steps. In a vibrational-coupling step (Figure 8a), the proton-donating (W_{D1}) and proton-accepting (W_A) water molecules in the first hydration shell were vibrationally coupled with the C6−O6 and O6−H6 stretching modes, respectively (Figure 6). These couplings enhanced the markedly large amplitudes of the C6−O6 and O6−H6 stretching vibrations. Then, in an intramolecular-energy-transfer step (Figure 8b), the excess energy appeared to be transferred into a torsional motion, resulting in a conformational change.

Let us offer a possible explanation for the second step in our proposed mechanism (i.e., the intramolecular energy transfer from the stretching modes into a hydroxymethyl rotational motion). In liquid H_2O, it is possible that O−H stretching-mode vibrational energy can relax into the H−O−H bending mode via the vibrational resonance (the Fermi resonance) with the overtone of the bending mode, which is a special feature of liquid H_2O.[62] In contrast, the efficiency of this process decreases for other systems such as liquid HDO, D_2O, and alcohols, because of a significant decrease in the overlap between the O−H stretching mode and the overtone of the bending mode.[62] This mechanism holds for the C6−O6−H6 fragment in glucopyranose, because of the same frequency mismatch between the O6−H6 stretching mode and the overtone of the C6−O6−

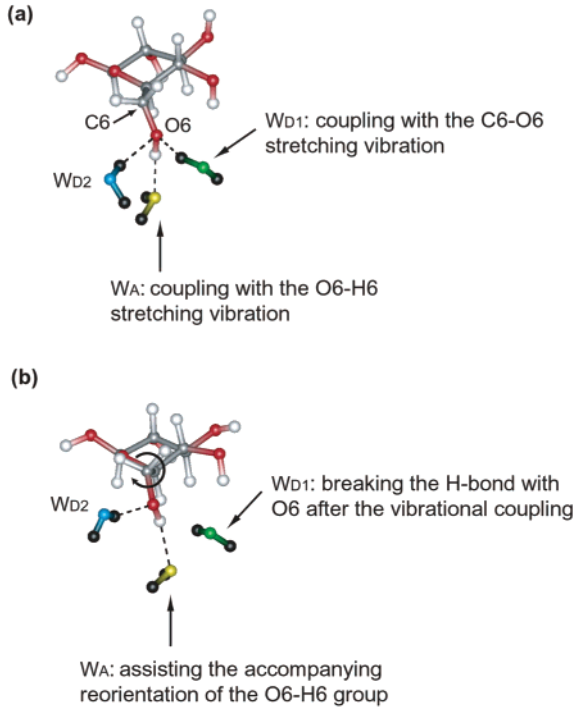

Figure 8. Schematic illustration of a vibrational-resonance-triggered reorientation in the hydroxymethyl group of β-glucopyranose in water (from the T to G^+ conformer). The two snapshots were taken from the ab initio MD trajectory. The three water molecules in the first hydration shell are colored yellow (W_A, a proton acceptor), green (W_{D1}, a proton donor), and blue (W_{D2}, a proton donor), respectively, while hydrogens are colored black. The other water molecules are omitted here. The dashed lines denote hydrogen bonds. In the β-glucopyranose molecule, carbon atoms are colored gray, oxygens red, and hydrogens white. Part a shows a vibrational-coupling step. W_{D1} and W_A induced the markedly large C6−O6 and O6−H6 stretching vibrations, respectively (for more detail, see Figures 6−8). Part b shows an intramolecular-energy-transfer step. The induced stretching-mode vibrational energies appeared to be transferred intramolecularly into a torsional motion of the hydroxymethyl rotation (the discussion is given in the text). After the vibrational coupling with the C6−O6 stretching vibration was finished, W_{D1} broke the hydrogen bond with O6 in a short period (see green line at ∼4.0 ps in Figure 3c); W_{D2} might guide the direction of the hydroxymethyl reorientation. In contrast, W_A continued the hydrogen bond with O6 (Figure 3b), assisting the accompanying reorientation of the O6−H6 group (Figures 4b and 4d).

H6 bending mode. In addition to this, the vibrational relaxation from the C6−O6 stretching mode into the C6−O6−H6 bending mode is also probably inhibited, because the C6−O6 stretching-mode frequency (about 900−1000 cm^{-1}) is lower by about 500 cm^{-1} than the C6−O6−H6 bending-mode frequency (about 1500 cm^{-1}). Therefore, as a consequence, the excess vibrational energy of the simultaneously highly excited O6−H6 and C6−O6 stretching modes appeared to be intramolecularly transferred into a torsional motion of the hydroxymethyl group, resulting in a conformational change (Figure 8b). In fact, it was experimentally observed that excitation of the O−H stretch leads to isomerization in 2-fluoroethanol;[63] it was also experimentally shown that excitation of the N−H stretch leads to isomerization in *N*-acetyl-tryptophan methyl amide.[64]

After the vibrational-coupling period was finished, W_{D1} moved away from O6 (see 4.1−4.5 ps in Figure S3 in the Supporting Information), whereas W_{D2} might guide the direction of the hydroxymethyl rotation from the T to the G^+ conformer. At the same time, W_A continued the hydrogen bond with O6 (Figure 3b), assisting the accompanying reorientation of the O6−H6 group (Figures 4b and 4d). However, since this was primarily due to the remarkably strong hydrogen bond between H6 and O_A, as we discussed (see also Figures 3 and 4), its role appeared to be of secondary importance for the process of the reorientation for the hydroxymethyl torsion angle. Also, the slower reorientation (during 5.8−6.6 ps) of the O6−H6 group after this process might be merely rearranged toward a more favored arrangement of hydrogen bonds around the hydroxymethyl group. However, these reorientations of the O6−H6 group could be regarded as part of the intramolecular vibrational energy relaxation.

Although we compared the instantaneous amplitudes for the C6−O6−H6 bending vibration during the pretransition period with those during the transition period, we could not find a significant feature in going from the pretransition to the transition period (Figure S4 in the Supporting Information). This implies that the C6−O6−H6 bending mode was not critically involved in the intermolecular vibrational energy transfer studied here. In addition, we found that the vibrational frequency of the torsional motion of the hydroxymethyl groups was normally much lower: in simulations ii−vi, about 87−97% of the frequencies for the torsion angle of the hydroxymethyl groups were concentrated in the frequency region below 300 cm^{-1}, which are lower than librational motions of liquid water in the 300−1000 cm^{-1} region. This probably suggests that vibrational couplings between the torsional motion of the hydroxymethyl group and librational motions of liquid water are rather difficult and therefore considered to be less important in our study of the reorientation of the hydroxymethyl group.

Is the amount of the vibrational energy of these stretching vibrations induced by the vibrational couplings reasonably enough to overcome the potential barrier for the hydroxymethyl rotation? To address this question quantitatively, we estimated the vibrational energies of the C6−O6 and O6−H6 stretching vibrations, respectively, by simply computing $E^{vib}_{C-O} = {}^1/_2\mu_{C-O}(dD_{6,3}/dt)^2$ and $E^{vib}_{O-H} = {}^1/_2\mu_{O-H}(dD_{3,1}/dt)^2$, where $D_{6,3}$ and $D_{3,1}$ are the detail coefficients associated with the third band at the sixth level obtained from the time series of the C6−O6 distance and the first band at the third level obtained from the time series of the O6−H6 distance, respectively (these frequency bands correspond to the C6−O6 and O6−H6 stretching vibrations, respectively), and μ_{C-O} and μ_{O-H} are reduced masses for the C6−O6 and O6−H6 systems, respectively. Because of an underestimate of vibrational frequencies owing to the CPMD method within the BLYP functional, we used a scaling factor of 1.21 (1.1 × 1.1) for the vibrational energies (within a harmonic approximation, vibrational energy is proportional to the square of its vibrational frequency).

During 3.4−3.8 ps (the pretransition period), the vibrational energies of both the C6−O6 and the O6−H6 stretching vibrations were significantly increased (Figure 9). These were due to the remarkably large amplitudes of the C6−O6 and O6−H6 stretching vibrations induced by the vibrational couplings, as we discussed (Figures 4 and 6). In this region, the energies simultaneously exceeded about 3 kcal mol^{-1} (about 5 times larger than the thermal energy, i.e., ∼0.59 kcal mol^{-1}) (Figures 9a and 9b), indicating that the total vibrational energy presumably exceeded roughly 6 kcal mol^{-1}. This value is comparable to typical values for the potential barriers between hydroxymethyl rotamers of glucopyranose recently estimated by quantum chemical calculations,[65] i.e., 3.7−5.8 kcal mol^{-1} (note, however, that accurate evaluation of the potential barriers between hydroxymethyl rotamers is still a delicate task; reported values for the barriers range from about 2 to 6 kcal mol^{-1}. See also refs 11, 15, 19, 20, 22, and 23), suggesting that the total

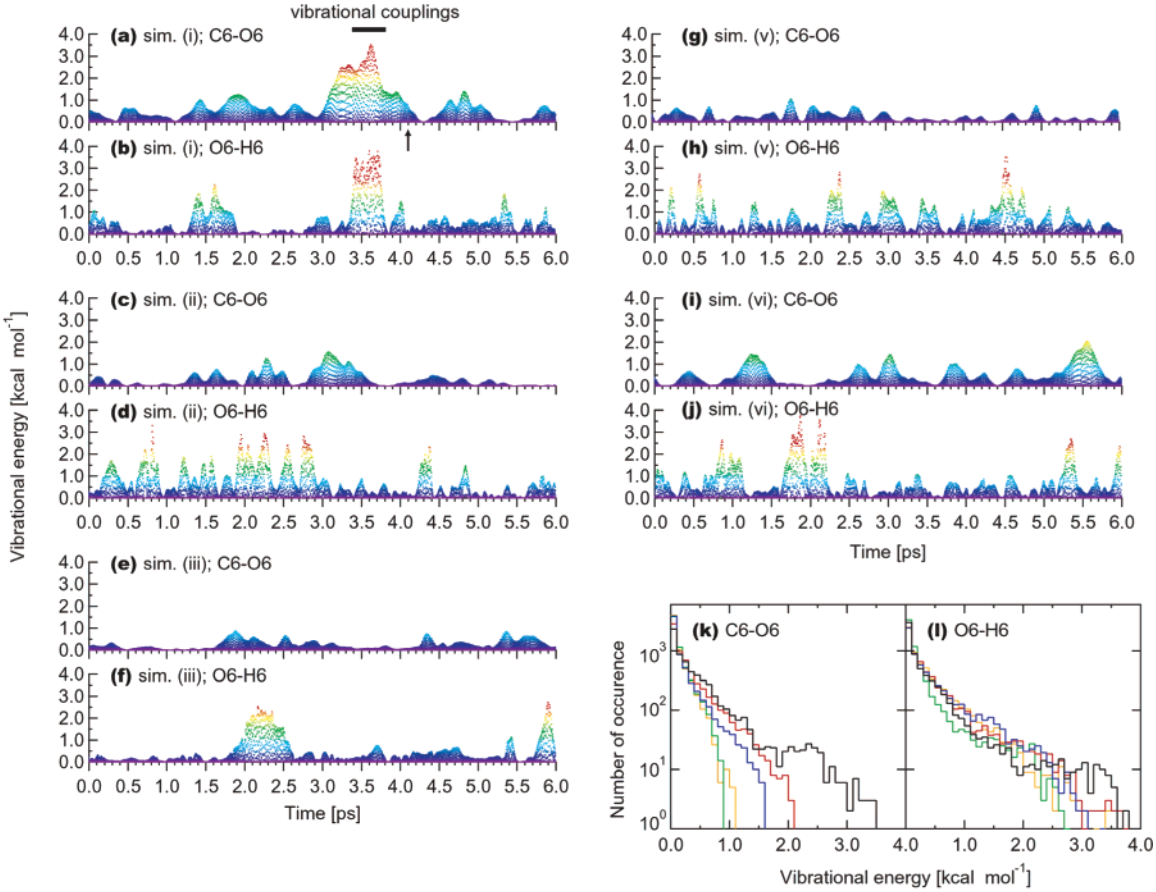

Figure 9. Time evolution of the estimated vibrational energies for the C6−O6 and O6−H6 stretching vibrations and their distributions. The time evolution of the C6−O6 and O6−H6 stretching-mode vibrational energies in the MD trajectory that underwent the reorientation of the hydroxymethyl group (simulation i) is shown in parts a and b, respectively (for the entire period (0−8.2 ps), see Figure S5 in the Supporting Information). The arrow in part a denotes the start point of the transition from Tg^- to G^+g^+ (about 4.12 ps). The bar in part a indicates the markedly strong vibrational couplings (see also Figure 6). In parts c−j, the time evolution of the C6−O6 and O6−H6 stretching-mode vibrational energies in the MD trajectories that did not undergo a rotational transition is shown: part c (C6−O6) and part d (O6−H6), simulation ii; part e (C6−O6) and part f (O6−H6), simulation iii; part g (C6−O6) and part h (O6−H6), simulation v; part i (C6−O6) and part j (O6−H6), simulation vi. Parts k and l show the distributions of the C6−O6 and O6−H6 stretching-mode vibrational energies, respectively: black, simulation i; blue, simulation ii; green, simulation iii; yellow, simulation v; red, simulation vi. For our estimates of the vibrational energies, see the text. All distributions were obtained by considering the NVE simulations of 6 ps.

vibrational energy induced by the vibrational couplings was possibly enough to overcome the potential barrier. Consistently, the remarkable decreases of the vibrational energies of the C6−O6 and O6−H6 stretching vibrations suggest that both the vibrational energies were substantially transferred into a torsional motion of the hydroxymethyl group, resulting in a conformational change (see ∼4.3 ps in Figures 9a and 9b).

In addition, we calculated the vibrational energies of the C6−O6 and O6−H6 stretching vibrations in the trajectories that did not undergo a rotational transition. In these cases, the C6−O6 and O6−H6 stretching-mode vibrational energies hardly exceeded about 2 and 3 kcal mol^{-1}, respectively (see Figures 9k and 9l, respectively), suggesting that the total vibrational energies in these cases could not exceed potential barriers needed for the reorientation of the hydroxymethyl group. None of the simulations ii−vi underwent a simultaneous increase in the vibrational energy of the C6−H6 and O6−H6 stretching vibrations. In particular, the C6−O6 stretching-mode vibrational frequencies were not significantly enhanced in these cases (Figures 9c, 9e, 9g, and 9i).[66] This implies that a highly excited C6−O6 stretching vibration may play an important role in rotational transitions in the hydroxymethyl group. However, which of the O6−H6 and C6−O6 stretching modes played a more critical role in the reorientation is unclear. The lesser enhancements of the C6−O6 stretching-mode vibrational energies in Figures 9c, 9e, 9g, and 9i appear to be linked to the nature of the vibrational density of states of liquid water; since the density of states of liquid water at ∼1000 cm^{-1} is small compared with 3000 cm^{-1}, the vibrational coupling of liquid water with the C−O stretch (around ∼1000 cm^{-1}) is considered to be a less frequent occurrence compared with the vibrational coupling with the O−H stretch.

To explain why these vibrational couplings happened (Figures 9a and 9b), we compared the hydrogen-bonding properties of the hydroxymethyl group in the MD trajectory that underwent the transition with those in the MD trajectories that did not. Although a conventional way to examine the hydration structure around the hydroxymethyl group is to calculate the sugar oxygen−water oxygen pair correlation function, such investigation is not suited for our present study, because this kind of analysis does not distinguish proton-donating and proton-accepting water molecules. Here, we attempted a different approach; we separately investigated hydrogen-bonding properties of proton-donating and proton-accepting water molecules.

First, using all of the MD trajectories, we examined the relationship between the O6−C6−O_d angle and the O6···O_d distance, where O_d is an oxygen atom of a first-hydration-shell water molecule acting as a proton donor to O6. To do this, we classified the region for the O6−C6−O_d angle (θ_d) into three categories: $0° < \theta_d \leq 25°$ (nearly parallel); $25° < \theta_d \leq 35°$

TABLE 2: Hydration Effects of Proton-Donating Water Molecules[a] on the Standard Deviations for the C6−O6 Bond

simulation[b]	standard deviation (Å)	population for θ_d (the O6−C6−O_d angle) (%)		
		$\theta_d \le 25°$	$25° < \theta_d \le 35°$	$\theta_d > 35°$
i[c]	0.0486	31	12	57
ii	0.0357	5	38	57
iii	0.0327	7	12	81
iv	0.0318	2	1	97
v	0.0349	5	36	59
vi	0.0410	19	29	52

[a] The criteria for proton-donating first-hydration-shell water molecules were the O6−H−O_d angle ≥120° and the O6···O_d distance <3.3 Å, where O_d is an oxygen atom of a first-hydration-shell water molecule acting as a proton donor to O6. [b] For the conformation, see the Simulation Models and Methods section. [c] The data were obtained by averaging 0−6 ps.

(moderately parallel); $\theta_d > 35°$ (not parallel). The average O6···O_d distance in the 0−25° region (nearly parallel) (2.975 Å) was longer by about 0.08 Å than that averaged over the other two categories (2.893 Å). This indicates that, when the C6−O6 and C6−O_d vectors are almost parallel, hydrogen bonds between O6 and proton-donating water molecules typically tend to be slightly weaker.

In fact, W_{D1} (nearly parallel) and W_{D2} (not parallel) (Figure 8) formed weaker and stronger hydrogen bonds, respectively; the average O6···O_{D1} and O6···O_{D2} distances during 2.0−4.5 ps were 3.035 and 2.906 Å, respectively. This was also confirmed by calculating the distances between O6 and the centers of the maximally localized Wannier functions associated with the two lone-pair orbitals of O6 that hydrogen-bonded with W_{D1} and W_{D2}; the average distances were 0.315 and 0.337 Å, respectively, indicating that W_{D1}, the one that was vibrationally coupled with the C6−O6 stretching motion, formed a weaker hydrogen bond with O6 compared with W_{D2}. This weaker hydrogen bond is partly because, since one lone-pair orbital of O6 was strongly pulled out by W_{D2}, the other lone-pair orbital was not significantly pulled out.

Besides, we examined the relationship between the population distribution of the three categories and the fluctuations of the C6−O6 bond. When 31% and 19% of the O6−C6−O_d angles were lower than 25° (nearly parallel) (simulations i and vi, respectively), the standard deviations for the C6−O6 bond were higher (0.0486 and 0.0410 Å, respectively) than those in the other simulations (Table 2). In contrast, when 97% of the O6−C6−O_d angles were higher than 35° (not parallel) (simulation iv), the standard deviation for the C6−O6 bond was the smallest (0.0318 Å) (Table 2). These imply that a proton-donating water molecule in the situation where the C6−O6 and C6−O_d vectors are almost parallel plays a role in enhancing the fluctuations of the C6−O6 bond.

To clarify this point further, we calculated the distributions of the O6−C6−O_d angles for all of the simulations and compared the distribution for the pretransition period in simulation i with those that did not undergo a rotational transition (simulations ii−vi). The results show that the distribution for the pretransition period (2−4 ps) is significantly different from those obtained from the trajectories that did not undergo a rotational transition (Figures 10b and 10c). The distribution for the pretransition period (2−4 ps) is characterized by two peaks: one centered on about 15° and the other centered on about 50° (the orange line in Figure 10b). The former and latter peaks are attributed to W_{D1} and W_{D2}, respectively. However, the distribution for the posttransition period (6−8.2 ps) is rather similar to those shown in Figure 10c and is notably different

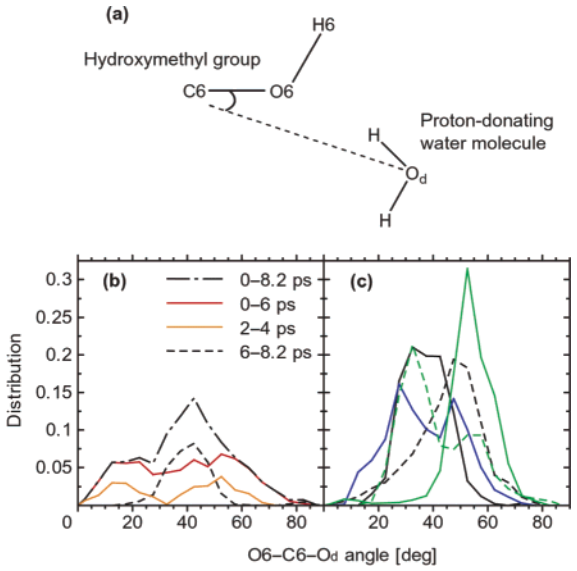

Figure 10. Distributions of the O6−C6−O_d angles. Part a shows the definition of the O6−C6−O_d angle. The criteria for proton-donating first-hydration-shell water molecules were the O6−H−O_d angle ≥120° and the O6···O_d distance <3.3 Å. Part b shows the distributions of the O6−C6−O_d angles in the trajectory of simulation i, which underwent the reorientation of the hydroxymethyl group for four different periods: the orange line, 2−4 ps (the pretransition period); the red line, 0−6 ps; the black dashed line, 6−8.2 ps (the posttransition period); the black dash−dotted line, 0−8.2 ps (the entire period). Part c shows the distributions of the O6−C6−O_d angles in the trajectories that did not undergo a hydroxymethyl rotational transition: the black solid line, G^+t; the black dashed line, G^+g^-; the green solid line, G^-g^+; the green dashed line, G^-t; the blue solid line, Tg^-.

TABLE 3: Hydration Effects of Proton-Accepting Water Molecules[a] on the Standard Deviations for the O6−H6 Bond

simulation[b]	standard deviation (Å)	O6···O_a distance[c] (Å)	H6···O_a distance[c] (Å)
i[d]	0.0285	2.862	1.896
ii	0.0335	2.750	1.765
iii	0.0245	2.917	1.970
iv	0.0290	2.854	1.907
v	0.0320	2.783	1.797
vi	0.0317	2.774	1.784

[a] The criteria for proton-accepting first-hydration-shell water molecules were the O6−H6−O_a angle ≥120° and the H6···O_a distance <2.4 Å. [b] For the conformation, see the Simulation Models and Methods section. [c] O_a denotes an oxygen atom of a first-hydration-shell water molecule that acts as a proton acceptor to O6. [d] The data were obtained by averaging 0−6 ps.

from that for the pretransition period (see the orange and dashed black lines in Figure 10b). The analysis probably suggests that the observed vibrational coupling was associated with the hydration structure around the hydroxymethyl group.

Second, we analyzed the hydrogen-bonding properties of proton-accepting water molecules. To do this, we examined the relationship between the fluctuations of the O6−H6 bond and the hydrogen-bonding properties of proton-accepting water molecules. The standard deviations for the O6−H6 distances increased with decreasing the average O6···O_a distance (and thus the average H6···O_a distance), where O_a is an oxygen atom of a first-hydration-shell water molecule acting as a proton acceptor to O6 (Table 3). This indicates that the fluctuations of the O6−H6 bond were mainly created by a resonant intermolecular OH stretching vibration between the O6−H6 group and proton-accepting water molecules, because, the shorter the average hydrogen bond is, the more the rate of the vibrational

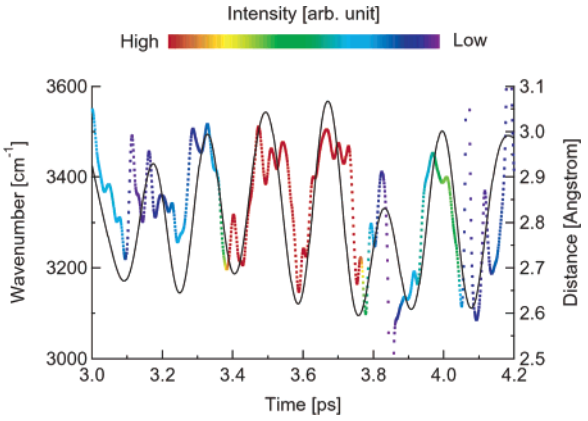

Figure 11. Modulation of the instantaneous O6−H6 stretching-mode frequencies by the O6···O_A distance during the pretransition period. The time series of the O6···O_A distance (black line) was smoothed by cutting off frequency components above about 300 cm^{-1}; that is, the black line is the sum of two components associated with the zeroth and first frequency bands at the seventh level. For the time-frequency spectrum for the O6−H6 stretching-mode vibration during 2−5 ps, see also Figure 6a.

resonance increases. This interpretation is probably supported by an experimental study by Woutersen and Bakker.[67]

What is special for the pretransition period in simulation i is that the time length of the high vibrational resonance between the O6−H6 group and W_A was longer than those of the other cases (simulations ii−vi) (Figure 9). How was this persistence of the resonant intermolecular OH stretching-mode maintained? To address this issue, we also investigated the low-frequency dynamics for this trajectory and found that the low-frequency dynamics (about 200 cm^{-1}) was also involved in the pretransition period (Figure S6a in the Supporting Information). In hydrogen-bonded systems, this low-frequency dynamics (about 150−200 cm^{-1}) is primarily attributed to hydrogen-bonded O···O stretching motions.[60a] Thus, predictably, the above finding was also confirmed by comparing the instantaneous O6−H6 stretching-mode frequencies with the time series of the O6···O_A distance; the comparison shows that the instantaneous frequencies were modulated by the low-frequency dynamics of the hydrogen bond (Figure 11). This modulation is because the OH stretching-mode frequencies in hydrogen-bonded systems depend on the hydrogen-bonded O···O distances.[68] Hence, these findings mean that the O6−H6 group was vibrationally coupled not only with the resonant OH stretching vibration but also with the low-frequency dynamics of the hydrogen bond between O6 and O_A. For the other trajectories that did not undergo any transition, we could not find such clear, prolonged vibrational coupling to the low-frequency region synchronizing the strong O6−H6 stretching vibration (Figure S6 in the Supporting Information).

The time length of the strong vibrational coupling between the O6−H6 stretching mode and W_A is about 400 fs (Figure 11). The value is about 4−8 times longer than an extremely fast relaxation time of resonant intermolecular energy transfer in liquid water (50−100 fs), in which the resonant OH stretching mode plays a significant role.[67,69,70] This somewhat longer persistence of the vibrational coupling had three possible origins: (1) the additional vibrational coupling of the low-frequency dynamics of the hydrogen bond between O6 and W_A (Figure S6a in the Supporting Information; Figure 11); (2) their stronger microscopic polarization interaction compared with that between water molecules in the liquid phase, as we mentioned; (3) the smaller number of water molecules into which the system of the O6−H6 group and W_A could transfer their resonant vibrational energy using the OH stretching mode (and possibly the overtone of the H−O−H bending mode) (i.e., 2) compared with that for a pair of vibrationally resonant water molecules in the liquid phase (i.e., 3). However, the typical time length of vibrational couplings that could lead to reorientations of hydroxymethyl groups is unclear from the present analysis.

Ultrafast energy relaxation in liquid water[67,69−71] (less than 100 fs) implies that this time scale is too fast to affect most chemical reactions[72] and may rather play a role stabilizing biological molecules.[71] At the same time, this implies (1) that water is an extremely good conductor of vibrational energy via its OH groups[72] and (2) that water molecules may play an important role in transporting vibrational energy from one biological molecule containing OH groups to another.[67,72] Since our system consists of a glucopyranose only and water molecules, our observation is linked to the former. The present work not only suggests that vibrational resonance between a CH_2OH-group-containing biomolecule and water molecules occurs in aqueous solution but also sheds light on an active role of resonant vibrational energy transfer in biomolecule−water systems, in which resonant vibrational energy transfer of liquid water, together with its vibrational resonance with the C−O stretch, may even lead to a conformational change.

Although we carefully monitored the MD trajectory that underwent the reorientation of the hydroxymethyl group, no significant feature was found for water molecules hydrogen-bonded to the three first-hydration-shell water molecules during the simulation. Therefore, water molecules in the second hydration shell did not appear to play an active role in the observed vibrational couplings; they played a secondary role in the formation of the particular hydrogen-bonding of the three first-hydration-shell water molecules. This may be supported by recent theoretical studies that suggest that the dynamics of vibrational energy relaxation and intermolecular energy transfer is primarily determined by local solute−solvent interactions.[73−75] From a more technical point of view, studying second-hydration-shell water molecules was unavoidably limited in the present work, owing to the modest size of the supercell that we used.

In closing, we discuss the validity and limitation of our proposed mechanism. First, whether our mechanism can be applied to other hydroxymethyl rotational transitions is an important issue. Of course, we investigated the transition from the T to G^+ rotamer only and did not investigate either the transition between G^+ and G^- or the one between G^- and T. This is because, owing to the limited numbers and lengths of our ab initio simulations, we could not obtain MD trajectories involving these transitions. This is not surprising because a recent study by Kirschner and Woods shows that the lifetime for the G^- conformer is about 5 ns in water.[22] This time scale is beyond typical time scales for ab initio MD simulations that present-day computers can afford. However, since intramolecular vibrational energy transfer is a fundamental process, if a similar hydration structure is formed (however, because of the complexity of the hydrogen-bond network of liquid water, possible hydrogen-bond patterns associated with the resonant vibrational coupling may not be limited to the one characterized by Figures 8 and 10b) and strong vibrational coupling that could overcome the potential barriers occurs, then the same mechanism is considered to be relevant for the other rotational transitions. However, the rate of the mechanism could depend on the hydroxymethyl rotamers because (1) the hydration structure of the hydroxymethyl group perhaps depends on the hydroxymethyl rotamers and (2) the potential barrier depends on the hydroxymethyl rotamers.

Second, another important question is how dominant our mechanism is in aqueous solution, which is not apparent from the present study. There may be other possible mechanisms. For example, a possible variant mechanism that might be derived from the present study is that, when a C−O stretch and/or an O−H stretch in a hydroxyl group other than the hydroxymethyl group in a glucopyranose molecule is vibrationally highly excited, the excess energy could similarly be transferred into a hydroxymethyl conformational change; however, the energy could much more easily be transferred into rotational motions of the OH group and possibly into the fluctuations of the sugar puckering. Another possible mechanism is that the highly excited C6−O6−H6 bending vibration by neighboring water molecules could be transferred into a hydroxymethyl conformational change, because, in a gas-phase simple molecule, intramolecular energy interconversion between bending vibration and torsional motion is in principle possible.[76] However, this scenario may be minor or unlikely in aqueous solution, because of the frequency mismatch between the C6−O6−H6 bending mode and the H−O−H bending mode of liquid water. For example, the C−O−H bending-mode frequency of methanol in aqueous solution is lower by 200−250 cm^{-1} than the bending-mode frequency of liquid water[77] (note also that, since the bandwidths of both the bending modes are relatively narrow, the overlap of these modes is considerably small).

Third, let us comment on the limitation of theoretical approximations used for describing our proposed mechanism. Although Car−Parrinello MD simulations naturally include anharmonicity, nuclei are treated as classical particles. Therefore, quantum nuclear effects are not included in the present study. Furthermore, a quantum mechanical treatment of vibrational energy transfer for our mechanism could possibly be important. At the same time, we note that recent studies suggest that a classical treatment of vibrational energy relaxation provides a reasonable description for the one that is treated fully quantum mechanically,[78,79] which probably implies that our proposed mechanism is at least qualitatively valid.

Despite all this, our proposed mechanism may have implications for understanding the structural and conformational properties of oligo- and polysaccharides. Once the 1→6 glycosidic linkage is formed, resonant vibrational coupling in our proposed mechanism (Figure 8) is entirely prevented for this torsional angle. First, this in turn implies that the reorientation mechanism for the 1→6 glycosidic linkage in disaccharides may be qualitatively different from that in monosaccharides. Second, it implies that, upon the 1→6 linkage, the torsion angle associated with the linkage may become more difficult to rotate in aqueous solution than the one for the hydroxymethyl group and may be more stably retained even in the dynamic hydrogen-bond network of liquid water. In fact, the torsion angle associated with the (1→6)-linked branch is rigid in aqueous solution.[80]

Conclusions

First, our analysis suggests that the T conformer of glucopyranose has a small population (probably, roughly 10%) in aqueous solution and that the $G^-/G^+/T$ (gg/gt/tg) ratio of β-glucopyranose in aqueous solution is possibly about 30:60:10 (or about 35:55:10) rather than a ratio of about 55:45:0 that was originally estimated by Nishida and co-workers.[3] The reestimated experimental ratio is in good agreement with several computational studies[12,18,21,25] and the one experimentally determined by Thibaudeau et al.[8] for methyl β-glucopyranoside. The reestimated ratio of the hydroxymethyl rotamer populations for β-glucopyranose in aqueous solution may be used for tests and validations of molecular modeling of carbohydrates; however, further refinement of the ratio may be necessary both experimentally and theoretically.

This agreement probably partly explains the discrepancies in the population of the T conformer between theoretical and experimental studies that have been discussed in the literature.[12,18,21,25−27] Also, the present work suggests that reported negative populations of the T rotamer of glucopyranose derivatives in NMR studies[3b,4] are not only due to the inaccuracy of the Haasnoot−Altona curves[6] but also due to the assumption of the perfectly staggered conformations. In particular, the O5−C5−C6−O6 torsional angle in the T rotamer deviated considerably from its ideal value of 180°. It shifted by about 30° toward the value in the G^+ rotamer and hence away from that in the G^- rotamer. This also implies that the transition between the G^+ and the T rotamers is probably easier than that between the G^- and the T rotamers in β-glucopyranose in aqueous solution, which is in agreement with the recent very long MD simulation of methyl α-glucopyranoside in water.[22] While the lengths of our simulations are limited, our values for the torsion angle obtained by the ab initio MD simulations imply that care should be taken into account when one uses the perfectly staggered conformations for the hydroxymethyl torsion angle for the determination of the six limiting values of vicinal proton−proton coupling constants from Karplus-type equations in calculating hydroxymethyl rotamer populations in monosaccharides in solution.

Second, our time-frequency analysis of the MD trajectory that underwent the reorientation from the T to the G^+ rotamer shows that, before the reorientation, the O6−H6 stretching mode was vibrationally coupled with the proton-accepting first-hydration-shell water molecule, whereas the C6−O6 stretching mode was vibrationally coupled with the proton-donating one (Figure 8). The analysis also suggests that the vibrational energies of the C6−O6 and O6−H6 stretching modes induced by the above vibrational couplings were transferred intramolecularly into a torsional motion of the hydroxymethyl group, resulting in its reorientation. The amount of the induced total vibrational energy was estimated to be comparable to typical values for the potential barriers between hydroxymethyl rotamers of carbohydrates, suggesting that the vibrational energy was probably enough to overcome the potential barrier. Furthermore, the hydrogen-bonding properties of the hydroxymethyl group during the pretransition period in the MD trajectory that underwent the reorientation were significantly different from those in the MD trajectories that did not undergo a rotational transition.

These findings perhaps propose a simple but possible reorientation mechanism for the hydroxymethyl rotamers in glucopyranose in water: (1) resonant vibrational couplings of the C6−O6 and/or O6−H6 stretching modes with first-hydration-shell water molecules and (2) its intramolecular energy transfer from these stretching-mode vibrational energies into a torsional motion of the hydroxymethyl group. However, the rate of the mechanism could depend on the hydroxymethyl rotamers because (1) the hydration structure of the hydroxymethyl group perhaps depends on the hydroxymethyl rotamers and (2) the potential barrier depends on the hydroxymethyl rotamers. However, owing to the limited numbers and lengths of our ab initio simulations, our mechanism is far from complete and may be oversimplified. Nonetheless, our mechanism has implications for the structural and conformational properties of oligo- and polysaccharides. First, it implies that the reorientation mecha-

nism of the 1→6 glycosidic linkage in disaccharides may be qualitatively different from that in monosaccharides. Second, it implies that, upon the 1→6 linkage, owing to the absence of our proposed mechanism, the torsion angle associated with the linkage may become more difficult to rotate in aqueous solution than the one for the hydroxymethyl group and may be more stably retained even in the dynamic hydrogen-bond network of liquid water.

Third, the present study has important implications for how biological molecules surrounded by the hydrogen-bond network use (ultrafast) resonant vibrational energy transfer in liquid water. In particular, our analysis not only suggests that vibrational resonance between a CH_2OH-group-containing biomolecule and water molecules occurs in aqueous solution but also sheds light on an active role of resonant vibrational energy transfer in biomolecule−water systems, in which the resonant intermolecular vibrational energy transfer of liquid water, together with its resonance with the C−O stretch, may even lead to a conformational change. We believe that the present work has valuable insights into carbohydrate−water interactions.

Acknowledgment. Our ab initio simulations were performed on the Hitachi SR8000 supercomputer of Information Technology Center, The University of Tokyo.

Supporting Information Available: Hydroxymethyl rotamer populations for β-glucopyranose in D_2O using several sets of three values for the O5−C5−C6−O6 torsion angle, dependence of the population of the tg (T) rotamer of β-glucopyranose in D_2O on the three O5−C5−C6−O6 torsion-angle values used for determining the limiting values for $^3J_{H5,H6}$, time series of the C6−O6 and O6−H6 distances during −0.5 to 0.7 ps, time series of the O6−C6−O_{D1} and O6−C6−O_{D2} angles, time-frequency spectrum for the C6−O6−H6 bending mode in simulation i and the corresponding instantaneous amplitudes, time evolution of the estimated vibrational energies for the C6−O6 and O6−H6 stretching vibrations in simulation i for the entire region, and the role of the low-frequency dynamics in the prolonged strong O6−H6 stretching-mode vibrational energy during the pretransition period. This material is available free of charge via the Internet at http://pubs.acs.org.

References and Notes

(1) Imberty, A.; Pérez, S. *Chem. Rev.* **2000**, *100*, 4567.
(2) Duus, J. Ø.; Gotfredsen, C. H.; Bock, K. *Chem. Rev.* **2000**, *100*, 4589.
(3) (a) Nishida, Y.; Ohrui, H.; Meguro, H. *Tetrahedron Lett.* **1984**, *25*, 1575. (b) Nishida, Y.; Hori, H.; Ohrui, H.; Meguro, H. *J. Carbohydr. Chem.* **1988**, *7*, 239.
(4) Bock, K.; Duus, J. Ø. *J. Carboydr. Chem.***1994**, *13*, 513.
(5) Stenutz, R.; Carmichael, I.; Widmalm, G.; Serianni, A. S. *J. Org. Chem.* **2002**, *67*, 949.
(6) Haasnoot, C. A. G.; De Leeuw, F. A. A. M.; Altona, C. *Tetrahedron* **1980**, *36*, 2783.
(7) Roën, A.; Padrón, J. I.; Vázquez, J. T. *J. Org. Chem.* **2003**, *68*, 4615.
(8) Thibaudeau, C.; Stenutz, R.; Hertz, B.; Klepach, T.; Zhao, S.; Wu, Q.; Carmichael, I.; Serianni, A. S. *J. Am. Chem. Soc.* **2004**, *126*, 15668.
(9) Kroon-Batenburg, L. M. J.; Kroon, J. *Biopolymers* **1990**, *29*, 1243.
(10) Polavarapu, P. L.; Ewig, C. S. *J. Comput. Chem.* **1992**, *13*, 1255.
(11) Van Eijck, B. P.; Hooft, R. W. W.; Kroon, J. *J. Phys. Chem.* **1993**, *97*, 12093.
(12) Grootenhuis, P. D. J.; Haasnoot, C. A. G. *Mol. Simul.* **1993**, *10*, 75.
(13) Cramer, J. C.; Truhlar, D. G. *J. Am. Chem. Soc.* **1993**, *115*, 5745.
(14) Glennon, T. M.; Zheng, Y.-J.; Le Grand, S. M.; Shutzberg, B. A.; Merz, K. M., Jr. *J. Comput. Chem.* **1994**, *15*, 1019.
(15) Zuccarello, F.; Buemi, G. *Carbohydr. Res.* **1995**, *273*, 129.
(16) Cheetham, N. W. H.; Lam, K. *Carbohydr. Res.* **1996**, *282*, 13.
(17) Brown, J. W.; Wladkowski, B. D. *J. Am. Chem. Soc.* **1996**, *118*, 1190.
(18) Senderowitz, H.; Parish, C.; Still, W. C. *J. Am. Chem. Soc.* **1996**, *118*, 2078.
(19) Klewinghaus, P.; van Eijck, B. P.; Kouwijzer, M. L. C. E.; Kroon, J. *THEOCHEM* **1997**, *395*−*396*, 289.
(20) Wladkowski, B. D.; Chenoweth, S. A.; Jones, K. E.; Brown, J. W. *J. Phys. Chem. A* **1998**, *102*, 5086.
(21) Barrows, S. E.; Storer, J. W.; Cramer, C. J.; French, A. D.; Truhlar, D. G. *J. Comput. Chem.* **1998**, *19*, 1111.
(22) Kirschner, K. N.; Woods, R. J. *Proc. Natl. Acad. Sci. U.S.A.* **2001**, *98*, 10541.
(23) Kuttel, M.; Brady, J. W.; Naidoo, K. J. *J. Comput. Chem.* **2002**, *23*, 1236.
(24) Kony, D.; Damm, W.; Stoll, S.; van Gunsteren, W. F. *J. Comput. Chem.* **2002**, *23*, 1416.
(25) Corchado, J. C.; Sánchez, M. L.; Aguilar, M. A. *J. Am. Chem. Soc.* **2004**, *126*, 7311.
(26) Brady, J. W. *J. Am. Chem. Soc.* **1989**, *111*, 5155.
(27) Molteni, C.; Parrinello, M. *J. Am. Chem. Soc.* **1998**, *120*, 2168.
(28) (a) Tuckerman, M. E.; Laasonen, K.; Sprik, M.; Parrinello, M. *J. Phys. Chem.* **1995**, *99*, 5749. (b) Tuckerman, M. E.; Laasonen, K.; Sprik, M.; Parrinello, M. *J. Chem. Phys.* **1995**, *103*, 150.
(29) Marx, D.; Tuckerman, M. E.; Hutter, J.; Parrinello, M. *Nature* **1999**, *397*, 601.
(30) Tuckerman, M. E.; Marx, D.; Parrinello, M. *Nature* **2002**, *417*, 925.
(31) Percival, D. B.; Walden, A. T. *Wavelet Methods for Time Series Analysis*; Gill, R., Rippley, B. D., Ross, S., Williams, D., Eds.; Cambridge Series in Statistical and Probabilistic Mathematics; Cambridge University Press: Cambridge, U. K., 2000.
(32) Huang, N. E.; Shen, Z.; Long, S. R.; Wu, M. C.; Shih, H. H.; Zheng, Q.; Yen, N.-C.; Tung, C. C.; Liu, H. H. *Proc. R. Soc. London, Ser. A* **1998**, *458*, 903.
(33) Corzana, F.; Motawia, M. S.; Hervé du Penhoat, C.; Pérez, S.; Tschampel, S. M.; Woods, R. J.; Engelsen, S. B. *J. Comput. Chem.* **2004**, *25*, 573.
(34) Suzuki, T.; Sota, T. *J. Phys. Chem. B* **2005**, *109*, 12603.
(35) (a) Car, R.; Parrinello, M. *Phys. Rev. Lett.* **1985**, *55*, 2471. (b) Parrinello, M. *Solid State Commun.* **1997**, *102*, 107. (c) Marx, D.; Hutter, J. In *Modern Methods and Algorithms of Quantum Chemistry*; Grotendorst, J., Ed.; NIC, FZ: Jülich, Germany, 2000; pp 301−449. See also http://www.theochem.ruhr-uni-bochum.de/research/marx/cprev.en.html.
(36) (a) Hohenberg, P.; Kohn, W. *Phys. Rev.* **1964**, *136*, B864. (b) Kohn, W.; Sham, L. J. *Phys. Rev.* **1965**, *140*, A1133. (c) Parr, R. G.; Yang, W. *Density-Functional Theory of Atoms and Molecules*; Breslow, R., Goodenough, J. B., Halpern, J., Rowlingson, J. S., Eds.; The International Series of Monographs on Chemistry 16; Oxford University Press: New York, 1989.
(37) Parrinello, M. *Comput. Sci. Eng.* **2000**, *2*, 22.
(38) (a) Becke, A. D. *Phys. Rev. A* **1988**, *38*, 3098. (b) Lee, C.; Yang, W.; Parr, R. G. *Phys. Rev. B* **1988**, *37*, 785.
(39) Goedecker, S.; Teter, M.; Hutter, J. *Phys. Rev. B* **1996**, *54*, 1703.
(40) We used CPMD, version 3.7 (IBM Corp, 1990−2003, and Max-Plank-Institut für Festkörperforshung Stuttgart, 1997−2001), developed by J. Hutter et al.
(41) For values for the electronic fictitious mass, see (a) Grossman, J. C.; Schwegler, E.; Draeger, E. W.; Gygi, F.; Galli, G. *J. Chem. Phys.* **2004**, *120*, 300. (b) Kuo, I.-F. W.; Mundy, C. J.; McGrath, M. J.; Siepmann, J. I.; VandeVondele, J.; Sprik, M.; Hutter, J.; Chen, B.; Klein, M. L.; Mohamed, F.; Krack, M.; Parrinello, M. *J. Phys. Chem. B* **2004**, *108*, 12990.
(42) Martyna, G. J.; Klein, M. L.; Tuckerman, M. E. *J. Chem. Phys.* **1992**, *97*, 2635.
(43) Tuckerman, M. E.; Parrinello, M. *J. Chem. Phys.* **1994**, *101*, 1302.
(44) Huang, N. E.; Shen, Z.; Long, S. R. *Annu. Rev. Fluid Mech.* **1999**, *31*, 417.
(45) (a) Lai, Y.-C. *Phys. Rev. E* **1998**, *58*, R6911. (b) Lai, Y.-C.; Armbruster, D.; Kostelich, E. J. *Phys. Rev. E* **2000**, *62*, R29.
(46) Phillips, S. C.; Gledhill, R. J.; Essex, J. W.; Edge, C. M. *J. Phys. Chem. A* **2003**, *107*, 4869.
(47) Suzuki, T.; Kawashima, H.; Kotoku, H.; Sota, T. *J. Phys. Chem. B* **2005**, *109*, 12997.
(48) Cummings, D. A. T.; Irizarry, R. A.; Huang, N. E.; Endy, T. P.; Nisalak, A.; Ungchusak, K.; Burke, D. S. *Nature* **2004**, *427*, 344.
(49) Olhede, S.; Walden, A. T. *Proc. R. Soc. London, Ser. A* **2004**, *460*, 955.
(50) Walden, A. T.; Contreras Cristán, A. *Proc. R. Soc. London, Ser. A* **1998**, *454*, 2243.
(51) Daubechies, I. *Ten Lectures on Wavelets*; CBMS−NSF Regional Conference Series in Applied Mathmatics 61; Society for Industrial and Applied Mathematics: Philadelphia, PA, 1992.
(52) Csonka, G. I.; Kolossváry, I.; Császár, P.; Éliás, K.; Csizmadia, I. G. *THEOCHEM* **1997**, *395*−*396*, 29.

(53) Rockwell, G. D.; Grindley, T. B. *J. Am. Chem. Soc.* **1998**, *120*, 10953.

(54) Jeffrey, G. A.; McMullan, R. K.; Takagi, S. *Acta Crystallogr., Sect. B* **1977**, *33*, 728.

(55) Brown, G. M.; Levy, H. A. *Acta Crystallogr., Sect. B* **1979**, *35*, 656.

(56) Marchessault, R. H.; Pérez, S. *Biopolymers* **1979**, *18*, 2369.

(57) (a) Marzari, N.; Vanderbilt, D. *Phys. Rev. B* **1997**, *56*, 12847. (b) Silvestrelli, P. L.; Marzari, N.; Vanderbilt, D.; Parrinello, M. *Solid State Commun.* **1998**, *107*, 7.

(58) Marzari, N.; Souza, I.; Vanderbilt, D. *Psi-K Newsletter* **2003**, *57*, 129. See http://psi-k.dl.ac.uk.

(59) (a) Silvestrelli, P. L.; Parrinello, M. *Phys. Rev. Lett.* **1999**, *82*, 3308. (b) Silvestrelli, P. L.; Parrinello, M. *J. Chem. Phys.* **1999**, *111*, 3572.

(60) In the present work, the term *stretching vibration*, if it is used for a pair of hydrogen-bonded oxygen atoms, indicates a relative motion of the two hydrogen-bonded atoms along the hydrogen-bond axis. In the field of the low-frequency dynamics study of liquid water (or more generally, liquid systems), this motion is often referred to as an O···O stretching vibration (or a longitudinal motion). See, for example, (a) Padró, J. À.; Martí, J. *J. Chem. Phys.* **2003**, *118*, 452. (b) Idrissi, A.; Longelin, S.; Sokolić, F. *J. Phys. Chem. B* **2001**, *105*, 6004. (c) Silvestrelli, P. L.; Bernasconi, M.; Parrinello, M. *Chem. Phys. Lett.* **1997**, *277*, 478.

(61) What was especially found by our time-frequency analysis is that the time series of the O6···O_{D1} distance was characterized not only by a slow motion of about 150−200 cm^{-1} that is typically found in the low-frequency dynamics of liquid water but also by a higher-frequency component of about 900−1000 cm^{-1} (Figures 7a and 7b). Since C−O stretching-vibration frequencies are typically 900−1200 cm^{-1}, the latter can be interpreted as the vibrational coupling of the C6−O6 bond with O_{D1}. The vibrational coupling in the frequency region around 1000 cm^{-1} is not surprising because first-hydration-shell water molecules around glucopyranose play a role in reproducing infrared spectra of glucose in aqueous solution in 950−1200 cm^{-1}. See Suzuki, T.; Sota, T. *J. Chem. Phys.* **2003**, *119*, 10133.

(62) Dokter, A. M.; Woutersen, S.; Bakker, H. J. *Phys. Rev. Lett.* **2005**, *94*, 178301.

(63) Kafafi, Z. H.; Marquardt, C. L.; Shirk, J. S. *J. Chem. Phys.* **1989**, *90*, 3087.

(64) Dian, B. C.; Longarte, A.; Zwier, T. S. *Science* **2002**, *296*, 2369.

(65) Appell, M.; Strati, G.; Willett, J. L.; Momany, F. A. *Carbohydr. Res.* **2004**, *339*, 537.

(66) The time evolution of the O6−H6 and C6−O6 stretching-mode vibrational energies for simulation iv was not included in Figure 9, because of the following technical problem inherent to our time-frequency analysis. The time step for simulation iv is shorter than those for the other simulations (see the Simulation Models and Methods section), which means that the Nyquist frequency for the former is larger than that for the latter. Therefore, in going from a sampling interval of 0.968 to 0.822 fs, the third band at the sixth level (about the 889−1186 cm^{-1} region (values were scaled by a factor of 1.1)) shifts into about the 1046−1395 cm^{-1} region, which unavoidably prevented us from making a comparison. However, the fact that the standard deviation for the C6−O6 distance in simulation iv was the lowest (Table 2) suggests that the C6−O6 stretching-mode vibration in simulation iv was not significantly enhanced either.

(67) Woutersen, S.; Bakker, H. J. *Nature* **1999**, *402*, 507.

(68) Steiner, T. *Angew. Chem., Int. Ed.* **2002**, *41*, 48.

(69) Poulsen, J. A.; Nyman, G.; Nordholm, S. *J. Phys. Chem. A* **2003**, *107*, 8420.

(70) Backtorp, C.; Poulsen, J. A.; Nyman, G. *J. Phys. Chem. A* **2005**, *109*, 3105.

(71) Cowan, M. L.; Bruner, B. D.; Huse, N.; Dwyer, J. R.; Chugh, B.; Nibbering, E. T. J.; Elsaesser, T.; Miller, R. J. D. *Nature* **2005**, *434*, 199.

(72) Nitzan, A. *Nature* **1999**, *402*, 472.

(73) (a) Larsen, R. E.; Stratt, R. M. *J. Chem. Phys.* **1999**, *110*, 1036. (b) Deng, Y.; Ladanyi, B. M.; Stratt, R. M. *J. Chem. Phys.* **2002**, *117*, 10752.

(74) Vikhrenko, V. S.; Schwarzer, D.; Schroeder, J. *Phys. Chem. Chem. Phys.* **2001**, *3*, 1000.

(75) Graham, P. B.; Matus, K. J. M.; Stratt, R. M. *J. Chem. Phys.* **2004**, *121*, 5348.

(76) Schranz, H. W.; Collins, M. A. *J. Chem. Phys.* **1994**, *101*, 307.

(77) Van Erp, T. S.; Meijer, E. J. *Chem. Phys. Lett.* **2001**, *333*, 290.

(78) Bader, J. S.; Berne, B. J. *J. Chem. Phys.* **1994**, *100*, 8359.

(79) Fujisaki, H.; Straub, J. E. *Proc. Natl. Acad. Sci. U.S.A.* **2005**, *102*, 6726.

(80) Corzana, F.; Motawia, M. S.; Hervé du Penhoat, C.; van den Berg, F.; Blennow, A.; Pérez, S.; Engelsen, S. B. *J. Am. Chem. Soc.* **2004**, *126*, 13144.

(81) (a) Laaksonen, L. *J. Mol. Graphics* **1992**, *10*, 33. (b) Bergman, D. L.; Laaksonen, L.; Laaksonen, A. *J. Mol. Graph. Modell.* **1997**, *15*, 301. See also http://www.csc.fi/gopenmol.